System-Level Performance Evaluation of Downlink Non-orthogonal Multiple Access (NOMA)

Yuya Saito, Anass Benjebbour, Yoshihisa Kishiyama, and Takehiro Nakamura

Radio Access Network Development Department, NTT DOCOMO, INC.
3-5 Hikari-no-oka, Yokosuka, Kanagawa 239-8536 Japan

Abstract— **As a promising downlink multiple access scheme for further LTE enhancement and future radio access (FRA), this paper investigates the system-level performance of non-orthogonal multiple access (NOMA) with a successive interference canceller (SIC) on the receiver side. The goal is to clarify the potential gains of NOMA over orthogonal multiple access (OMA) such as OFDMA, taking into account key link adaptation functionalities of the LTE radio interface such as adaptive modulation and coding (AMC), hybrid automatic repeat request (HARQ), time/frequency-domain scheduling, and outer loop link adaptation (OLLA), in addition to NOMA specific functionalities such as dynamic multi-user power allocation. Based on computer simulations, we show under multiple configurations that the system-level performance achieved by NOMA is superior to that for OMA.**

Keywords – non-orthogonal multiple access, future radio access, successive interference canceller, Adaptive modulation and coding

I. INTRODUCTION

In order to continue to ensure the sustainability of 3GPP radio access technologies over the coming decade (LTE Release 12 and onwards), new solutions that can respond to future challenges need to be identified and developed [1, 2]. For future radio access (FRA) in the 2020s, significant gains in capacity and quality of user experience (QoE) are required in view of the anticipated exponential increase in the volume of mobile traffic, e.g., beyond a 500-1000 fold increase in the next decade. In cellular mobile communications, the design of radio access technology (RAT) is one important aspect in improving system capacity in a cost-effective manner. Radio access technologies are typically characterized by multiple access schemes, e.g., frequency division multiple access (FDMA), time division multiple access (TDMA), code division multiple access (CDMA), and OFDMA, which provide the means for multiple users to access and share the system resources simultaneously. In the 3.9 and 4th generation (4G) mobile communication systems such as Long-Term Evolution (LTE) [3] and LTE-Advanced [4, 5], standardized by the 3rd Generation Partnership Project (3GPP), orthogonal multiple access (OMA) based on OFDMA or single carrier (SC)-FDMA is adopted. The orthogonal design of multiple access is a reasonable choice for achieving good system-level throughput performance in packet-domain services with a simplified receiver design. However, in order to boost further the spectrum efficiency in the future, more advanced receiver designs are required in order to mitigate intra-cell and/or inter-cell interference. As a candidate multiple access for FRA including further LTE enhancement beyond Release 12, we proposed a downlink non-orthogonal multiple access (NOMA) where multiple users are multiplexed in the power-domain on the transmitter side and multi-user signal separation on the receiver side is conducted based on successive interference cancellation (SIC) [6-10]. From an information-theoretical point of view, it is well-known that non-orthogonal user multiplexing using superposition coding at the transmitter and SIC at the receiver not only outperforms orthogonal multiplexing, but also it is optimal in the sense of achieving the capacity region of the downlink broadcast channel [11]. In [6] and [7], system-level gains of NOMA were investigated based on the Shannon formula in the downlink and uplink. However, system-level performance employing actual link adaptation functionalities such as adaptive modulation and coding (AMC), hybrid automatic repeat request (HARQ), and time/frequency-domain scheduling is not reported yet to the best of our knowledge. In particular, accurate modulation and coding scheme (MCS) selection for SIC receiver is important to maximize the performance of NOMA with AMC. Therefore, this paper evaluates the downlink system-level performance gains of NOMA over OMA when applying AMC, HARQ, and scheduling, in addition to NOMA specific functionalities such as dynamic multi-user power allocation. Using computer simulations, under multiple configurations, it is shown that the overall cell throughput, cell-edge user throughput and the degree of proportional fairness achieved by NOMA are all superior to that of OMA. It is also shown that outer loop link adaptation (OLLA) for MCS selection provides further improvement of performance gain of NOMA using AMC.

The remainder of this paper is organized as follows. Section II describes the system model and the key functionalities utilized to introduce NOMA. In Section III after describing the employed system-level simulations, we provide and discuss the simulation results of the system-level performance of NOMA in comparison to that for OMA. Finally, Section IV concludes the paper.

II. DESCRIPTION OF NOMA WITH SIC

This section describes the system model and key functionalities utilized in NOMA for user multiplexing at the transmitter of the base station (BS) with SIC applied at the receiver of the user terminal (User Equipment (UE)). Throughout this paper, we assume a 1-by-2 SIMO system where the number of transmitter antennas at the BS is one ($N_t = 1$), while the number of receiver antennas at the UE is two ($N_r = 2$). There are K users per cell and the total transmit bandwidth, BW, is divided into S subbands, where the bandwidth of each subband is B ($BW = S \times B$). We assume that the multi-user scheduler selects m_s users from K then schedules a set of users, $U_s = \{i_s(1), i_s(2), ..., i_s(m_s)\}$, to subband s ($1 \leq s \leq S$), where $i_s(l)$ indicates the index of the l-th ($1 \leq l \leq m_s$) user scheduled at subband s, and m_s denotes the number of users non-orthogonally multiplexed at subband s. For the sake of simplicity, hereafter in this section, the time index, t, and the subcarrier index, f, are omitted and the channel coefficients are indicated as constants within each subband.

A. Signal Model

The transmit signal, x_s, at every subcarrier of subband s is a summation of the coded modulation symbol, $d_s(i_s(l))$, of the $i_s(l)$-th user. Thus, $d_s(i_s(l))$ of all m_s users are superposed as

$$x_s = \sum_{l=1}^{m_s} \sqrt{p_s(i_s(l))}\, d_s(i_s(l)), \quad (1)$$

where $E[|d_s(i_s(l))|^2] = 1$ and $p_s(i_s(l))$ is the allocated transmission power to user $i_s(l)$ at subband s. The N_r dimensional received signal

vector of user $i_s(l)$ at every subcarrier of subband s, $\boldsymbol{y}_s(i_s(l))$, is represented by

$$\boldsymbol{y}_s(i_s(l)) = \boldsymbol{h}_s(i_s(l))x_s + \boldsymbol{w}_s(i_s(l)), \quad (2)$$

where $\boldsymbol{h}_s(i_s(l))$ is the N_r-dimensional channel coefficient vector of user $i_s(l)$ at subband s, which includes distance dependent loss, shadowing loss, and instantaneous fading coefficients, and $\boldsymbol{w}_s(i_s(l))$ is the N_r-dimensional noise plus inter-cell interference vector of user $i_s(l)$ at subband s. Assuming that the receiver treats inter-cell interference as white noise, at the receiver maximal ratio combining (MRC) is applied to $\boldsymbol{y}_s(i_s(l))$ as follows:

$$\begin{aligned}\tilde{y}_s(i_s(l)) &= \boldsymbol{h}_s^{\boldsymbol{H}}(i_s(l))y_s(i_s(l))/\|\boldsymbol{h}_s\| \\ &= \sqrt{G_s(i_s(l))}x_s + n_s(i_s(l)) \\ &= \sqrt{G_s(i_s(l))}\sum_{k=1}^{m_s}\sqrt{p_s(i_s(k))}d_s(i_s(k)) \\ &\quad + n_s(i_s(l))\end{aligned} \quad (3)$$

where $G_s(i_s(l)) = \|\boldsymbol{h}_s(i_s(l))\|^2$ is the combining gain after MRC, while $n_s(i_s(l)) = \boldsymbol{h}_s^{\boldsymbol{H}}(i_s(l))\boldsymbol{w}_s(i_s(l))/\|\boldsymbol{h}_s\|$ is the noise plus inter-cell interference after MRC. The average power of $n_s(i_s(l))$ is denoted as $N_s(i_s(l)) = \mathrm{E}[|n_s(i_s(l))|^2]$. In the following, we define the channel gain of user $i_s(l)$ at subband s as $G_s(i_s(l))/N_s(i_s(l))$. In addition, we assume that the total transmission power per subband of the BS is common to all subbands and equal to P. Thus, for each subband s, the sum power constraint is represented by

$$\sum_{l=1}^{m_s} p_s(i_s(l)) = P. \quad (4)$$

At the receiver, U_s being the scheduled user set at subband s and user $i_s(l)$, $j \in U_s$, the scheduling signal-to-interference plus noise power ratio (SINR) at the receiver of each user, $i_s(l)$, is derived as in (5). We assume that the SIC receiver of user $i_s(l)$, is able to cancel perfectly and successively the interference from other user(s) j with channel gain $G_s(j)/N_s(j)$ lower than $G_s(i_s(l))/N_s(i_s(l))$. This assumption is reasonable because users with lower channel gains, as explained later, are allocated higher levels of transmit power than users with higher channel gains. Thus, they can be decoded at their corresponding receivers and the receivers of other users with higher channel gains. Note that the decoding and the successive cancellation order of signals from other users with higher channel gains are carried out in the order of the increasing channel gain. On the other hand, at the receiver of each user $i_s(l)$ the received signal from other user(s) j with channel gain $G_s(j)/N_s(j)$ higher than $G_s(i_s(l))/N_s(i_s(l))$ is treated as noise, thus no decoding nor cancellation of these users signals is performed. An example of the decoding and cancellation procedure for a 3-user NOMA case is illustrated in Fig. 1.

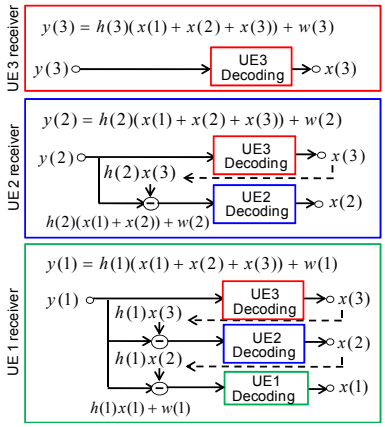

Fig. 1. Illustration of UE receivers for 3-user NOMA case (Channel gain order: UE1 > UE2 > UE3).

Given the aforementioned decoding and cancellation procedure, at the receiver of user $i_s(l)$, the SINR of user $i_s(l)$ at subband s, is represented as

$$SINR_s(i_s(l)|U_s) = \frac{G_s(i_s(l))p_s(i_s(l))}{\sum_{j\in U_s, \frac{G_s(i_s(l))}{N_s(i_s(l))} < \frac{G_s(i_s(j))}{N_s(i_s(j))}} G_s(i_s(l))p_s(j) + N_s(i_s(l))}. \quad (5)$$

In order to calculate the subband SINR of (5), the information on the transmit power allocated to each user is required. In the following, we explain the multi-user transmit power allocation that is employed.

B. *Dynamic multi-user Transmit Power Allocation*

In NOMA, the power allocation to one user affects the achievable throughput of not only that user but also the throughput of other users due to power-domain multi-user multiplexing. Therefore, multi-user transmit power allocation and multi-user scheduling are connected to each other. For the sake of simplicity, in this paper we assume disjoint power allocation and user scheduling where the power allocation for each candidate user set, U_s, is conducted first and then the scheduling metric is calculated. Even in this case, the optimal power allocation remains computationally complex because for each candidate user set all possible combinations of power allocations must be considered. Thus, in order to reduce further the computational complexity, we adopt a suboptimal fractional transmit power control (FTPC) that is similar to the transmission power control used in the LTE uplink [7]. With FTPC, the transmit power of user k in candidate user set U_s in subband s is dynamically allocated according to the channel gains of the multiplexed users as follows:

$$p_s(k) = \frac{P}{\sum_{j\in U_s}(G_s(j)/N_s(j))^{-\alpha_{FTPC}}}\left(\frac{G_s(k)}{N_s(k)}\right)^{-\alpha_{FTPC}}, \quad (6)$$

where α_{FTPC} ($0 \le \alpha_{FTPC} \le 1$) is the decay factor. The case of $\alpha_{FTPC} = 0$ corresponds to equal transmit power allocation among the users. The more α_{FTPC} is increased, the more power is allocated to the user with lower channel gain $G_s(k)/N_s(k)$. Note here that the same α_{FTPC} will be applied to all subbands and transmission times. Thus, the value of α_{FTPC} is an optimization parameter that needs to be determined *a priori* via computer simulations such that the target performance evaluation metric is maximized.

C. *Multi-user Scheduling and Candidate User Set Selection*

In NOMA, for each subband the scheduler allocates more than one user for simultaneous transmission. The scheduling metric that is adopted significantly affects the system capacity (measured by, for example, cell throughput) and user fairness (measured by, for example, cell-edge user throughput). The proportional fairness (PF) scheduler [12] is known to achieve a good balance between system capacity and user fairness by maximizing proportional fairness, i.e., the product of the average user throughput among all users within a cell. In [13], the multiuser scheduling version of the PF scheduler is presented and an approximated version is derived. In the approximated version, among all candidate user sets, the PF scheduling metric maximizing user set U_s is selected as follows:

$$\begin{aligned}Q_s(U) &= \sum_{k\in U}\left(\frac{R_s(k|U,t)}{L(k,t)}\right) \\ U_s &= \max_U Q_s(U)\end{aligned} \quad (7)$$

Term $Q_s(U)$ denotes the PF scheduling metric for candidate user set U, and it is given by the summation of the PF scheduling metric of all users in user set U. Term $R_s(k; t)$ is the instantaneous throughput of user k in subband s at time instance t (the time index of a subframe), whereas $L(k,t)$ is the average throughput of user k. When $t_c \gg 1$, which is valid in this paper as t_c is set to 200, (7) provides a good approximation of the multiuser proportional fairness scheduling

policy that maximizes the product of the average user throughput among the K users. In this paper, $L(k,t)$ is calculated as

$$L(k,t+1) = \left(1-\frac{1}{t_c}\right)L(k,t) + \frac{1}{S\times t_c}[\text{number of successively received bits}](k,t). \quad (8)$$

When throughput averaging time window t_c is set to 200 ms with the subframe length of 1 ms, the 200 ms average user throughput is measured. The throughput of user k in subband s at time instance t, the instantaneous user throughput $R_s(i_s(l)|U_s)$, is calculated based on the user SINR of (5) as follows.

$$R_s(i_s(l)|U_s)^{MCS^*} = SpectrumEfficiency^{MCS^*} \times \left(1-BLER^{MCS^*}|_{SINR_s(i_s(l)|U_s)}\right), \quad (9)$$

where

$$MCS^* = \max_{MCS} SpectrumEfficiency^{MCS} \times \left(1-BLER^{MCS}|_{SINR_s(i_s(l)|U_s)}\right). \quad (10)$$

Term $BLER^{MCS^*}$ denotes the block error rate (BLER) of the selected MCS corresponding to $SINR_s(i_s(l)|U_s)$ obtained from (5). For each candidate MCS, the corresponding $BLER_s(i_s(l)|U_s)^{MCS^*}$ is found first by checking the BLER vs. SINR curves obtained from link-level simulations. The achievable instantaneous user throughput of all candidate MCS sets is calculated, and the *MCS** set with the highest achievable instantaneous user throughput is selected. Note that the target BLER is set to 10% in the simulation. Term $R_s(i_s(l)|U_s)$ is set to zero if user k is not scheduled at subband s.

D. MCS Selection for Adaptive Modulation and Coding (AMC)

The LTE radio interface is used as baseline. Thus, we assume the same channel coding rate (including rate matching) and data modulation scheme over all the subbands allocated to each single user. MCS reselection for data transmission of each user is based on its average SINR over all the subbands allocated to it. Note that there is a mismatch between the MCS that is actually used for data transmission (based on SINR averaged over all allocated subbands) and the MCS used for user scheduling (based on subband SINR).

III. Simulation Evaluations

A. NOMA System-Level Simulations

We present system-level simulation results of the investigation on the performance gains of NOMA. The simulator used consists of a system-level model utilizing exponential SINR link-to-system level mapping [13]. The flow chart of the assumed system-level simulations is summarized in Fig. 1. From all K users, after channel and interference estimation at the receiver side, the channel gain is calculated and fed back to the BS. At the BS, assuming that all possible candidate user sets are searched, the number of candidate user sets is $V = \binom{K}{1} + \binom{K}{2} + \cdots + \binom{K}{m_s}$. For every subband s, the scheduling metric maximizing the candidate user set is selected. The scheduling metric is calculated based on the estimated instantaneous user throughput that is derived from subband SINR calculation after transmit power allocation as in (5). Once the user set scheduled for each subband is selected, the average SINR (in log-domain) of each user over its allocated subbands is derived. Based on this averaged SINR for each user, one MCS common to all allocated subbands is selected for each single user. At the UE receiver, the effective SINR is calculated for each user using EESM (exponential effective SNR mapping) model where the weighting factor beta is optimized for each MCS [14]. Based on the effective SINR, MCS decoding is attempted using the BLER vs. SINR link-level mapping table. If decoding is unsuccessful the SINR is stored in a buffer for possible chase combining with another future reception, whereas if the decoding is successful the UE throughput is updated accordingly by accumulating the newly received bits. We use chase combining as hybrid automatic repeat request (HARQ). Note that OMA is assumed to follow the same procedure as NOMA but with m_s = 1. When OLLA [15] is applied to OMA or NOMA, the threshold for MCS selection is adaptively adjusted by using outer-loop control based on acknowledgement (ACK)/Negative ACK (NACK) feedback from the UE as shown in Fig. 1. When ACK is received at the BS, the threshold for MCS selection is decreased by Δ_{step} x T_{BLER}; otherwise, when NACK is received, the threshold is increased by Δ_{step} x (1-T_{BLER}), where Δ_{step} and T_{BLER} indicate the step size of the threshold adjustment and the target BLER, respectively. In this paper, Δ_{step} and T_{BLER} are set to 0.5 and 10%, respectively.

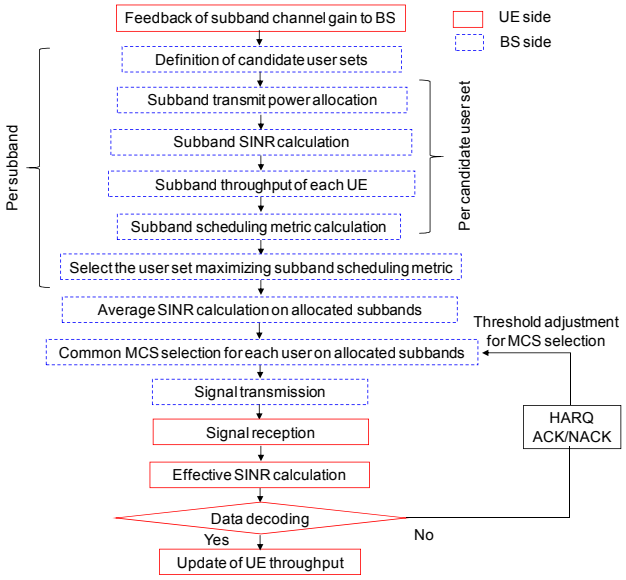

Fig. 1. Flow chart of NOMA system-level simulations.

B. Simulation Assumptions

To evaluate the performance gain of NOMA, a multi-cell system-level simulation is conducted. The simulation parameters are basically compliant with existing LTE/LTE-Advanced specifications [3-5]. We employed a 19-hexagonal macrocell model with 3 cells per cell site. The cell radius of the macrocells is set to 289 m (inter-site distance (ISD) = 500 m). K UEs are dropped randomly following a uniform distribution. In the propagation model, we take into account distance-dependent path loss with a decay factor of 3.76, lognormal shadowing with the standard deviation of 8 dB, and instantaneous multipath fading. The shadowing correlation between the sites (cells) is set to 0.5 (1.0). The spatial channel model (SCM) urban macro with a low angle spread is assumed [16]. The maximum Doppler frequency, f_D, is set to 5.55 Hz, which corresponds to 3 km/h at the carrier frequency of 2 GHz. The system bandwidth is 10 MHz and the total transmission power of the BS in each cell is 46 dBm. The antenna gain at the BS and UE is 14 dBi and 0 dBi, respectively. A one-antenna transmission and two-antenna reception (1-by-2 SIMO) system is assumed and a full buffer traffic model is used. For NOMA and OMA we assume the ideal channel and intra-cell/inter-cell interference estimation and unquantized feedback of the channel gain, but with a feedback delay such that the channel gain information is not available for scheduling until 4 subframes after the periodic report with a 2 ms interval. Also, in the evaluations we assume no

error propagation, thus SIC perfectly removes inter-user interference. The control delay of AMC is 4 ms and the round trip delay is 8 ms. In the evaluations, α_{FTPC} of 0.4 is used for FTPC. Table I summarizes the 20 modulation coding scheme (MCS) sets used for AMC. The simulation parameters are summarized in Table II. In order to investigate the performance gain of NOMA, the cell throughput and cell-edge user throughput are evaluated based on the following definitions. The cell throughput is defined as the average aggregated throughput for users scheduled per a single cell, while the cell-edge user throughput is defined as the 5% value of the cumulative distribution function (CDF) of the user throughput. As a metric to assess the degree of proportional fairness achieved among users we use the geometric mean of user throughput T of all K users.

$$F = \sqrt[K]{\prod_{k=1}^{K} T_k} \tag{11}$$

TABLE I. MCS SETS FOR AMC

Modulation Scheme	Channel Coding Rate										
QPSK	1/8	1/6	1/5	1/4	1/3	2/5	1/2	3/5	2/3	3/4	5/6
16QAM	1/2		3/5		2/3		3/4		5/6		
64QAM	3/5		2/3		3/4		4/5				

TABLE II. MAJOR SIMULATION PARAMETERS

Cell layout	Hexagonal grid, 19 sites, 3 cells per site
Inter-site distance	500 m
Minimum distance between UE and cell site	35 m
Distance dependent path loss	$128.1 + 37.6\log_{10}(r)$ dB
Shadowing standard deviation	8 dB
Correlation distance of shadowing	50 m
Shadowing correlation	0.5 (inter site) / 1.0 (intra site)
Channel model	3GPP Spatial Channel Model (SCM), Urban Macro
Channel estimation	Ideal
UE speed (Max. Doppler frequency)	3 km/h (5.55 Hz)
BS total transmission power	46 dBm
Transmit antenna gain & cable loss	14 dBi
UE antenna gain	0 dBi
UE noise figure	9 dB
Thermal noise density	-174 dBm /Hz
Carrier frequency	2 GHz
System bandwidth	10 MHz
Number of transmitter antennas	1
Number of receiver antennas	2
Number of UEs per cell	K = 2,4,8,10
Maximum number of multiplexed UEs	1 (OMA), 2 or 3 (NOMA)
Number of subbands	S = 1,2,4,8
Scheduling algorithm	Proportional Fairness (PF)
Control delay in scheduling & AMC	4.0 ms
HARQ combining scheme	Chase Combining
Round trip delay	8.0 ms
Channel gain reporting interval	2 ms
Traffic model	Full buffer model
α_{FTPC}	0.4

C. *Simulation Results*

First, the performance gain of NOMA over OMA is investigated for S = 1, i.e., wideband scheduling for OMA and wideband user multiplexing for NOMA. Figure 2 provides the CDF of the user throughput for OMA (m=1) and NOMA with the maximum multiplexing order of m = 2 and m = 3 for the number of UEs per cell of K = 10. The performance gains in the overall cell throughput and cell-edge user throughput for NOMA over OMA for m = 2 (m = 3) are approximately 27% (28%) and 34% (39%), respectively. Note that for NOMA substantial performance gains are obtained for cell center users in particular because they benefit more from being allocated more frequency or time resources.

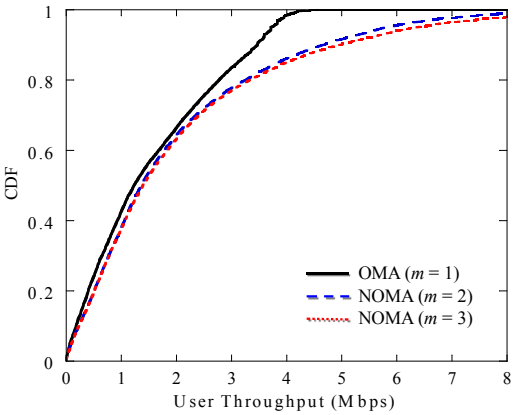

Fig. 2. CDF of user throughput for OMA (m = 1) and NOMA (m = 2 or 3) with S = 1 and K = 10.

The overall cell throughput gain and the ratio of 1-UE and 2-UE multiplexing for different numbers of UEs per cell are summarized in Table III. The table shows that as the number of UEs per cell is increased, the gain of NOMA is increased. The table also shows that the ratios for 1-UE and 2-UE multiplexing are almost 50% when the number of UEs per cell is 2, while the ratio for 2-UE multiplexing increases to approximately 90% when the number of UEs is 10.

TABLE III. PERFORMANCE GAIN AND UE RATIO OF NOMA FOR DIFFERENT NUMBERS OF UES PER CELL

Number of UEs per Cell (K)	Overall Cell Throughput Gain [%]	Ratio of 1-UE/2-UE Multiplexing [%]
2	11	53
4	21	77
8	26	87
10	27	89

Figure 3 shows the CDF of the absolute value of the difference in the channel gain (dB) between the 2 paired UEs of NOMA (m = 2) but for different numbers of UEs per cell. The difference in the channel gain increases as the number of UEs per cell is increased. Thus, more pairs of users with large differences in the channel gain (consequently higher gains for NOMA) can be scheduled.

Next, we investigate the throughput performance of NOMA with different numbers of subbands: S = 1, 2, 4, and 8. NOMA gains for different numbers of subbands are summarized in Table IV. The gains of NOMA in terms of overall cell throughput, cell-edge throughput, and degree of proportional fairness (geometric mean throughput) are reduced compared to those for OMA as the number of subbands is increased. This is due to two reasons: OMA has higher frequency-domain scheduling with larger number of subbands, and NOMA achieves lower multiplexing gains since the user transmit power allocation is per subband while the MCS selection remains wideband. Thus, with larger number of subbands, subband MCS selection would be required to achieve larger gains for NOMA with subband scheduling.

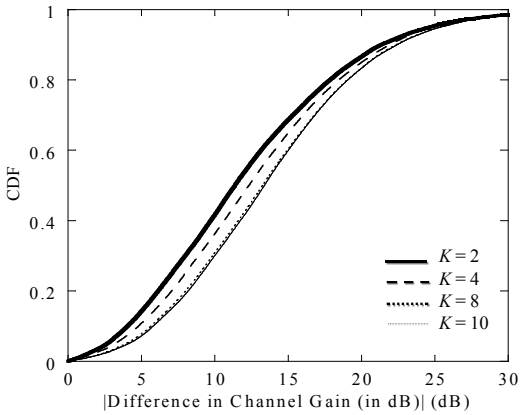

Fig. 3. CDF of difference in channel gains (in dB) between NOMA paired UEs, with $S = 1$ and $m = 2$.

TABLE IV. PERFORMANCE GAIN FOR DIFFERENT NUMBERS OF SUBBANDS

Number of Subbands (S)	Overall Cell Throughput Gain [%]	Cell-Edge Throughput Gain [%]	Geometric Mean Throughput Gain [%]
1	27	28	22
2	26	28	20
4	23	22	17
8	19	15	13

Finally, we investigate the performance of NOMA with OLLA. Figure 4 shows the CDF of user throughput for NOMA with $S = 1$, $m = 2$, and $K = 10$, with and without OLLA. As a comparison, the performance of OMA ($m = 1$) with and without OLLA is also plotted in the figure. The performance gains in the overall cell throughput and cell-edge user throughput for NOMA with OLLA over OMA with OLLA are approximately 24% and 26%, respectively. The dynamic transmit power control for NOMA impacts the accuracy of the threshold adjustment for MCS selection; therefore, the OLLA gains are slightly reduced for NOMA compared to those for OMA. To further improve the gains of NOMA with OLLA, further optimization of the step size of OLLA could be beneficial.

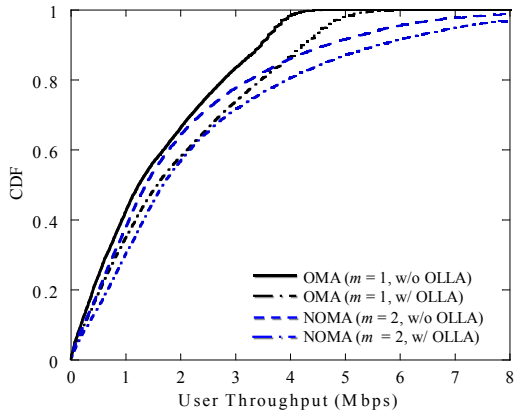

Fig. 4. CDF of user throughput with and without OLLA for OMA ($m = 1$) and NOMA ($m = 2$), with $S = 1$ and $K = 10$.

IV. CONCLUSION

We evaluated the system-level performance of NOMA taking into account more practical aspects of the cellular system and some of the key parameters and functionalities of the LTE radio interface such as frequency-domain scheduling, AMC, HARQ and OLLA, in addition to NOMA specific functionalities such as dynamic multi-user power allocation. Using computer simulations, we showed that the overall cell throughput, cell-edge user throughput, and the degree of proportional fairness of NOMA are all superior to that for OMA. This is because NOMA has more degrees of freedom to co-schedule more users in the same subband. However, the order of the gains depends on multiple factors such as the number of UEs per cell and the number of subbands for scheduling. In particular, wideband MCS selection is seen as a limiting factor to harnessing the benefits of subband user multiplexing for NOMA. It was also found that OLLA also improves the overall cell throughput and cell-edge user throughput of NOMA, even when dynamic power allocation is applied. Further optimizations of dynamic transmit power allocation and MCS adaptation for NOMA require further study.

REFERENCES

[1] NTT DOCOMO, "Requirements, candidate solutions & technology roadmap for LTE Rel-12 onward," 3GPP RWS-120010, June 2012.

[2] Y. Kishiyama, A. Benjebbour, H. Ishii, and T. Nakamura, "Evolution concept and candidate technologies for future steps of LTE-A," *IEEE ICCS2012*, Nov. 2012.

[3] 3GPP TS36.300, Evolved Universal Terrestrial Radio Access (E-UTRA) and Evolved Universal Terrestrial Radio Access Network (E-UTRAN); Overall description.

[4] 3GPP TR36.913 (V8.0.0), "Requirements for further advancements for E-UTRA (LTE-Advanced)," June 2008.

[5] 3GPP TR36.814 (V9.0.0), "Further advancements for E-UTRA physical layer aspects," Mar. 2010.

[6] K. Higuchi and Y. Kishiyama, "Non-orthogonal access with random beamforming and intra-beam SIC for cellular MIMO downlink," *IEICE RCS2012-89*, vol. pp. 85-90, July 2012.

[7] Y. Endo, Y. Kishiyama, and K. Higuchi, "A study on transmission power control considering inter-cell interference for non-orthogonal access with MMSE-SIC in cellular uplink," *IEICE RCS2012-46*, pp. 19-24, June 2012.

[8] J. Umehara, Y. Kishiyama, and K. Higuchi, "Enhancing user fairness in non-orthogonal access with successive interference cancellation for cellular downlink," *Proc. of ICCS*, Nov. 2012.

[9] N. Otao, Y. Kishiyama, and K. Higuchi, "Performance of non-orthogonal access with SIC in cellular downlink using proportional fair-based resource allocation," *Proc. of ISWCS*, pp. 476-480, Aug. 2012.

[10] Y. Saito, Y. Kishiyama, A. Benjebbour, T. Nakamura, A. Li, and K. Higuchi, "Non-orthogonal multiple access (NOMA) for future radio access," *Proc. of IEEE VTC spring 2013*, June 2013.

[11] D. Tse and P. Viswanath, *Fundamentals of Wireless Communication*, Cambridge University Press, 2005.

[12] F. P. Kelly, A. K. Maulloo, and D. K. H. Tan, "Rate control for communication networks: shadow prices, proportional fairness and stability," *Journal of the Operational Research Society*, vol. 49, Sept. 1998.

[13] M. Kountouris and D. Gesbert, "Memory-based opportunistic multi-user beamforming," *Proc. IEEE Int. Symp. Information Theory (ISIT)*, Adelaide, Australia, Sept. 2005.

[14] K. Brueninghaus, D. Astely, T. Salzer, S. Visuri, A. Alexiou, S. Karger, and G. A. Seraji, "Link performance models for system level simulations of broadband radio access systems," *Proc. IEEE PIMRC*, Sept. 2005.

[15] J. Lee, R. Arnott, K. Hamabe, and N. Takano, "Adaptive modulation switching level control in high speed downlink packet access transmission," *3G Mobile Communication Technologies*, pp. 156-159, May 2002.

[16] 3GPP, "Physical layer aspects for Evolved UTRA," TR 25.814,V7.1.0, Oct. 2006.